Pergamon

J. Mech. Phys. Solids, Vol. 46, No. 12, pp. 2303–2322, 1998
© 1998 Elsevier Science Ltd. All rights reserved
Printed in Great Britain
0022–5096/98 $—see front matter

PII: S0022–5096(98)00011–8

A CONSTITUTIVE MODEL FOR THE NON-SHOCK IGNITION AND MECHANICAL RESPONSE OF HIGH EXPLOSIVES

JOEL G. BENNETT,* KEITH S. HABERMAN, JAMES N. JOHNSON, BLAINE W. ASAY AND BRYAN F. HENSON

Los Alamos National Laboratory, Los Alamos, New Mexico 87544

(*Received* 5 *August* 1997; *in revised form* 12 *January* 1998)

ABSTRACT

An understanding of the non-shock ignition properties of energetic particulate composite materials, "high explosives" such as PBX-9501 is an important part of the safety assessments for conventional handling (transportation, storage, etc.) of weapons systems including assembly operations. This paper develops and demonstrates the use of a numerical constitutive model for PBX-9501 that includes viscoelastic response, statistical fracture mechanics, and an ignition hot-spot mechanism. The intent is that this model can be used in safety analyses involving accidents to prevent undesirable dispersion of Pu. The parameters have been determined that will predict the mechanical response and ignition/non-ignition of a set of experiments that have explored the non-shock properties of this material. © 1998 Elsevier Science Ltd. All rights reserved.

Keywords: microcracking, chemical-mechanical processes, constitutive behaviour, finite elements, energetic materials.

1. INTRODUCTION

The class of materials known as plastic (polymer) bonded explosives (PBX) is represented in this paper by PBX-9501. This material is a heterogeneous explosive consisting of 95 wt% HMX (octahydro-1,3,5,7-tetranitro-1,3,5,7-tetrazocine) crystals embedded in a binder consisting of 50% estane (a polyurethane) and 50% BDNPA/F (bis (2,2-dinitropropyl) acetal/bis (2,2-dinitropropyl) formal, 50/50 wt%). The HMX crystals are bi-modal in size distribution with the formulation of 71.25 wt% Class 1 HMX (84–96% smaller than 297 μ) and 23.75 wt% (75% smaller than 44 μ), which is a 3 : 1 course/fine ratio. The explosives are pressed from moulding powders and the microstructure, shown in the photograph of Fig. 1 represents an unusual challenge in engineering material modeling.

Nevertheless, the understanding and prediction of the non-shock ignition of energetic particulate composite materials is an area that is important in safety assessments of handling and assembly of weapons systems. Work in this area has received attention

* To whom correspondence should be addressed, Tel: 001 505 667 7888; Fax: 001 505 665 2137; E-mail: jbennett@lanl.gov

since the discovery in the early 1980s that mild mechanical shocks in solid propellants could lead to explosions that approach the violence of those produced by strong shock waves in the process known as SDT, Shock to Detonation Transition (Jensen, Bloomer and Brown, 1981; Green, *et al.*, 1981). These explosions, caused by mild multi-dimensional mechanical shocks, are referred to as non-shock ignition. In general, the investigation of this phenomenon has focused on experimental determinations of "go–no/go" conditions for ignition associated with impact velocity conditions, with limited effort made to identify the underlying causes of this ignition, which is attributed to micromechanical causes. Bonnett and Butler (1996) present a good summary of the current thinking in the literature.

2. HOT SPOT MECHANISMS

Although there are several proposed micromechanical processes that may be responsible, it is generally agreed upon that "non-shock" ignition occurs because of an isolated high-temperature region in the material called a "hot-spot". It is also generally agreed that these regions are caused by the interaction of the stress or shock waves with defects in the material, and the formation of the hot-spot depends on the mechanical, thermal and chemical properties of the material. However, the dominant mechanism for producing the hot-spot has not been generally agreed upon. Viscous heating, localized plastic work, friction between grains, hydrodynamic void (pore) collapse with adiabatic heating of the entrapped gas, internal shear, and shock interaction at density discontinuities are some of the micromechanical mechanisms that have been suggested and investigated (Field, *et al.*, 1982; Field *et al.*, 1992; Field, 1992). It is very likely that all of these mechanisms can produce a hot-spot under certain circumstances. However, Dienes (1984) has done an order-of-magnitude analysis that shows that the mechanism for the largest contribution to potential heat generation is the frictional forces on shear crack surfaces. Shear cracking certainly occurs in these materials, such cracking having been observed in the experiments by Howe *et al.* (1985) and others, although the cracks are difficult to detect. Dienes (1996) has also demonstrated that including the effect of frictional heating within the context of his statistical crack mechanics model (SCRAM) can induce ignition. In the work here, we have leaned heavily upon the insight of Dienes and the SCRAM approach, but we have implemented a viscoelastic, isotropic SCRAM model with ignition that we believe is accurate and efficient in simulating the 3-dimensional mechanical response including the non-shock ignition of PBX-9501. By incorporating these models into an explicit finite element code (DYNA3D, Whirley and Englemann, 1993) the practical modeling of the HE (High Explosives) in safety analyses of systems, wherein the HE is a sub-model, but a very important part of the overall simulation, is feasible.

3. VISCO ELASTIC CRACKING CONSTITUTIVE MODEL (Visco-SCRAM)

This model is based on the work of Addessio and Johnson (1990) and combines a general n- component Maxwell visco-elasticity model combined with the SCRAM

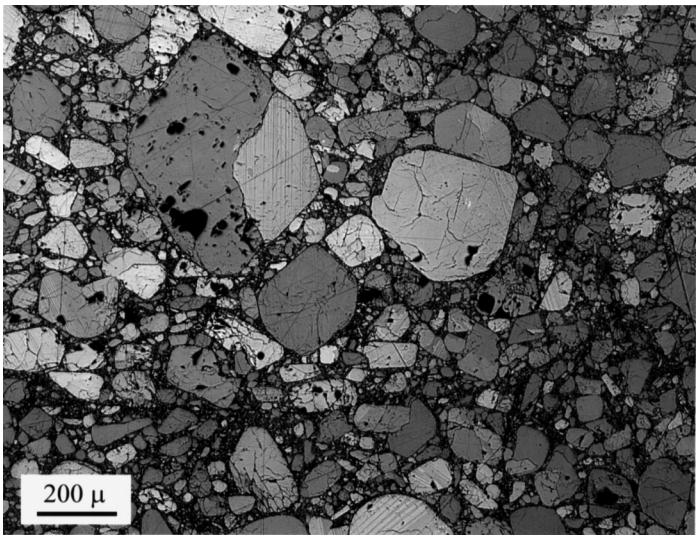

Fig. 1. A photomicrograph of PBX-9501 that shows the heterogeneous microstructure. (Courtesy of Cary Skidmore and David Phillips of the Los Alamos National Laboratory).

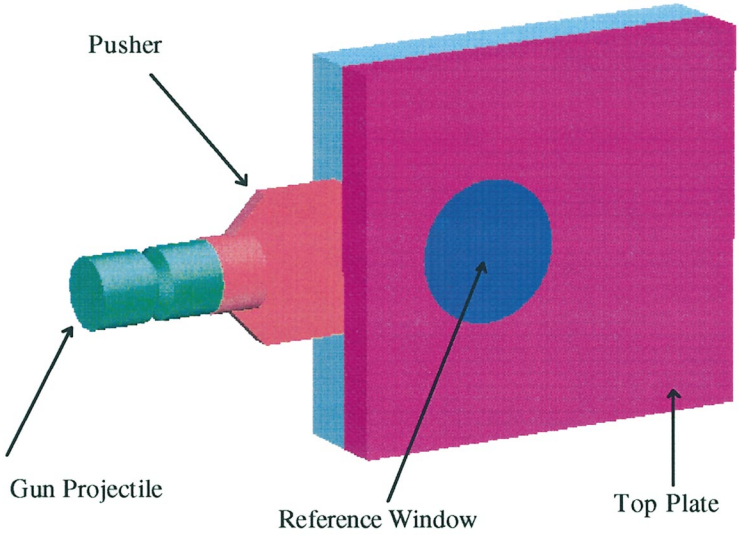

Fig. 12. Finite element model of the impact test.

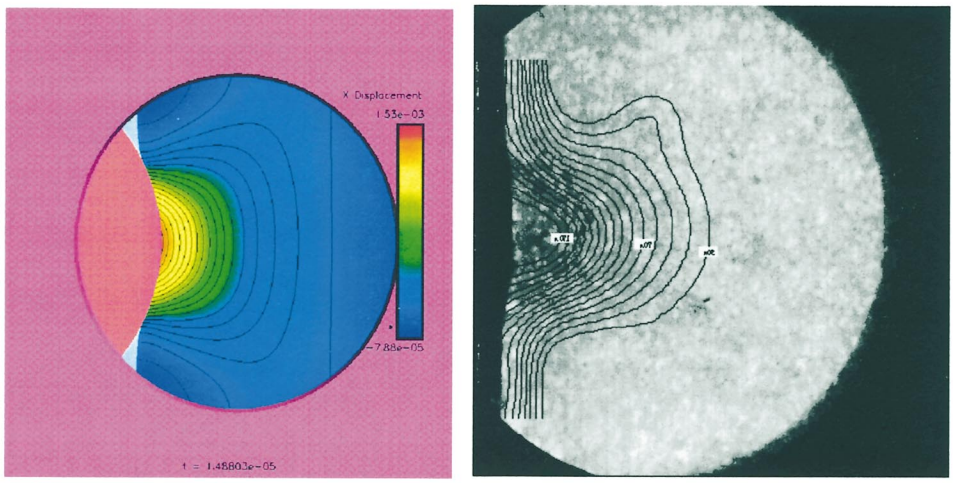

Fig. 13. A qualitative comparison of the calculated and experimental displacement fields.

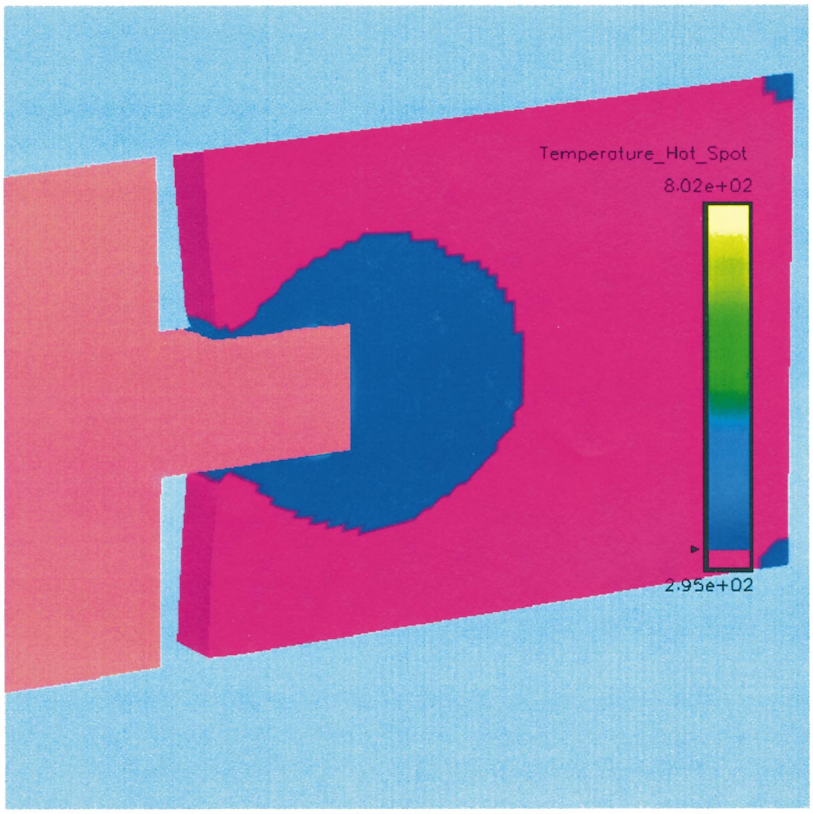

Fig. 15. Calculated hot spot temperature distribution.

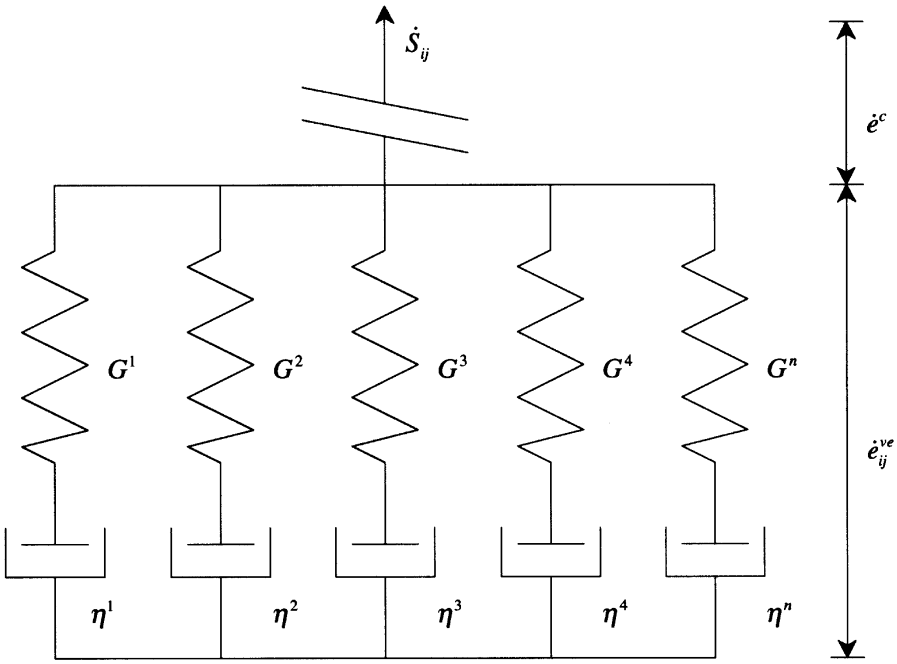

Fig. 2. A schematic diagram of the Visco-SCRAM model. $\dot{S}_{ij}$ is the deviatoric stress rate, $\dot{e}^{ve}_{ij}$ is the visco-elastic deviatoric strain rate, and $\dot{e}^c_{ij}$ is the deviatoric cracking strain rate. The G^n are the shear moduli, and the η^n are the damping constant for the nth component.

(Statistical Crack mechanics) approach of Dienes. SCRAM is a physically based micromechanical approach to the large deformation and cracking of brittle materials. During the deformation, the crack distribution is assumed to remain random, and the size of the distribution of the cracks is exponential. The model is shown schematically in Fig. 2.

Using Cartesian tensor index notation, the total strain rate for the solid is given by the kinematic relationship

$$\dot{\varepsilon}_{ij} = \tfrac{1}{2}\left(\frac{\partial \dot{u}_j}{\partial x_i} + \frac{\partial \dot{u}_i}{\partial x_j}\right)$$

where, x_i are the material point coordinates, and $\dot{u}_i$ are the material deformation rates in these coordinate directions, with the dotted variable indicating the time rate of change of that variable. The total strain rate can be decomposed into a deviatoric and mean strain rate as $\dot{\varepsilon}_{ij} = \dot{e}_{ij} + \delta_{ij}\dot{\varepsilon}_m$ with δ_{ij} being the Kronecker delta, and

$$\dot{\varepsilon}_m = \tfrac{1}{3}\dot{\varepsilon}_{ii}.$$

In the single spring-damper Maxwell model, with the relationship between the deviatoric stress and deviatoric strain in the elastic element is $S = 2Ge$ and the stress and strain rate in the viscous element is $S = 2\eta\dot{e}$, the stress rate is

$$\dot{S} = 2G\dot{e} - \frac{S}{\tau}$$

where $\tau = \eta/G$. Then, for the general viscoelastic solid (Fig. 2), with the deviatoric strain rates, $\dot{e}_{ij}^{ve}$, being in common and the deviatoric stresses for each component being additive, i.e.

$$S = \sum_{n=1}^{N} S^{(n)},$$

the general relationship between the deviatoric stress, stress rate, and strain rate is assumed to be

$$\dot{S}_{ij} = \sum_{n=1}^{N} \left(2G^{(n)} \dot{e}_{ij}^{ve} - \frac{S_{ij}^{(n)}}{\tau^{(n)}} \right) \tag{1}$$

The volumetric response rate is assumed to be given by, $\dot{\sigma}_m = K\dot{\varepsilon}_{ii}$, where K is the bulk modulus for the material. The total stress rate is the sum of the deviatoric and mean stress rates, $\dot{\sigma}_{ij} = \dot{S}_{ij} + \dot{\sigma}_m \delta_{ij}$.

The deviatoric strain rate in this model is the sum of the deviatoric visco-elastic strain rate and the deviatoric cracking strain rate

$$\dot{e}ij = \dot{e}_{ij}^{ve} + \dot{e}_{ij}^{c}. \tag{2}$$

The fundamental deviatoric cracking-strain versus deviatoric stress relationship is shown in Addessio and Johnson (1990) to be

$$e_{ij}^{c} = \beta^{e} c^{3} S_{ij}.$$

Here, c is the average crack radius, and β^{e} is a parameter relating the shear moduli and the initial crack distribution N_0 as

$$2G\beta^{e} = AN_0 \equiv \left(\frac{1}{a^3} \right).$$

with A being a constant and a the initial flaw size. With this definition, the relationship between the deviatoric strains and the crack radius is

$$2Ge_{ij}^{c} = \left(\frac{c}{a} \right)^3 S_{ij},$$

or, in rate form as

$$2G\dot{e}_{ij}^{c} = 3\left(\frac{c}{a} \right)^2 \frac{\dot{c}}{a} S_{ij} + \left(\frac{c}{a} \right)^3 \dot{S}_{ij}. \tag{3}$$

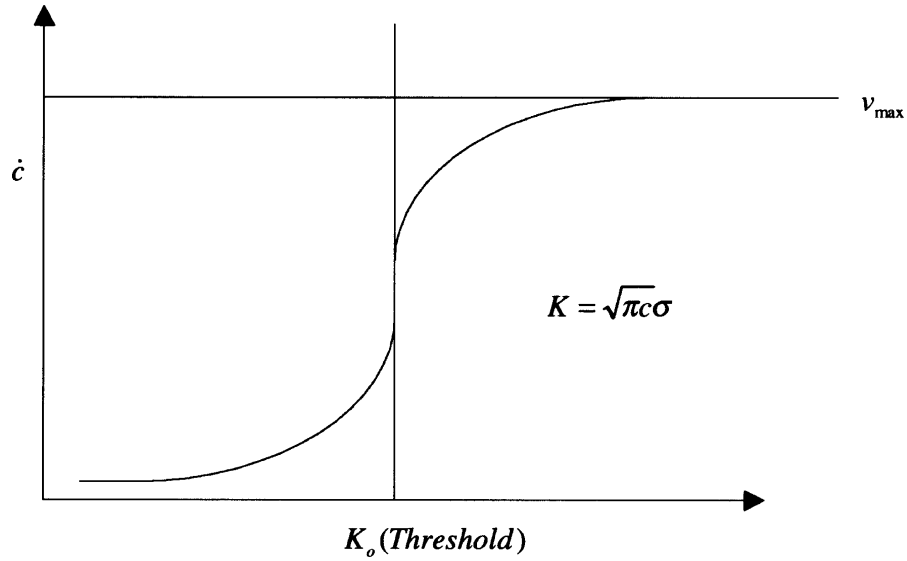

Fig. 3. The crack growth rate relationship shown schematically.

Using eqns 1–3, the deviatoric stress rate in the model is

$$\dot{S}_{ij} = \frac{2G\dot{e}_{ij} - \sum_{1}^{N} \frac{S_{ij}^{(n)}}{\tau^{(n)}} - 3\left(\frac{c}{a}\right)^3 \frac{\dot{c}}{a} S_{ij}}{1 + \left(\frac{c}{a}\right)^3}. \tag{4}$$

The stress rate in each Maxwell element is

$$\dot{S}_{ij}^{(n)} = 2G^{(n)}\dot{e}_{ij} - \frac{S_{ij}^{(n)}}{\tau^{(n)}} - \frac{G^{(n)}}{G}\left[3\left(\frac{c}{a}\right)^2 \frac{\dot{c}}{a} S_{ij} + \left(\frac{c}{a}\right)^3 \dot{S}_{ij}\right], \tag{5}$$

where

$$G = \sum_{1}^{N} G^{(n)}.$$

An evolution equation for the crack growth rate is required to complete this part of the model. Based on the work of Dienes (1996) we assume the crack growth rate depends on the stress intensity as shown schematically in Fig. 3.

This behaviour may be described by

$$\dot{c} = v_{\max}\left(\frac{K}{K_1}\right)^m \quad K < K'$$

$$\dot{c} = v_{\max}\left[1-\left(\frac{K_0}{K}\right)^2\right] \quad K \geqslant K'$$

where,

$$K' = K_0\sqrt{1+\left(\frac{2}{m}\right)}$$

and

$$K_1 = K_0\sqrt{1+\left(\frac{2}{m}\right)}\left[1+\frac{m}{2}\right]^{\frac{1}{m}}.$$

This visco-SCRAM model with five Maxwell components has been fitted to experimental data ranging over 8 orders of magnitude in relaxation times to determine the viscoelastic constants. Values of Young's modulus are obtained from ultrasonic (Olinger, 1982), Hopkinson bar (Gray, 1996), and quasi-static (Wiegand, 1996) measurement. The data extend over approximately eight decades of strain rate. Relaxation times for a generalized Maxwell model are obtained from the relationship that relaxation times are approximately one-tenth the reciprocal strain rate of the experimental test. A least-squares fit to the data is obtained in the form

$$E = [m_1 \log_{10}\tau + m_2(\log_{10}\tau)^2 + m_3]$$

where, $m_1 = -0.17077$, $m_2 = 0.026825$, and $m_3 = 7.1679$ for E in MPa and τ in seconds. Figure 4 shows the experimental data for the relaxation time and the fit to the data for PBX-9501. All of the material parameters for PBX-9501 associated with this model are given in Tables 1–3.

With these evolution equations and these parameters, the stress rate is found and integrated over the time step to give the updated state of stress within an element, a standard procedure for an explicit finite element code.

The stress-strain response predicted by this implementation of the visco-SCRAM constitutive equations into DYNA3D for a sample of PBX-9501 under a uniaxial load is shown in Fig. 5 for three different rates of deformation. These curves closely match the available experimental data for PBX-9501 at or near these strain rates.

4. HOT SPOT MODEL

Figure 6 shows an arbitrarily oriented micro-crack in a brittle solid under a pressure load and shear load along the crack face. In the SCRAM model, it is assumed that

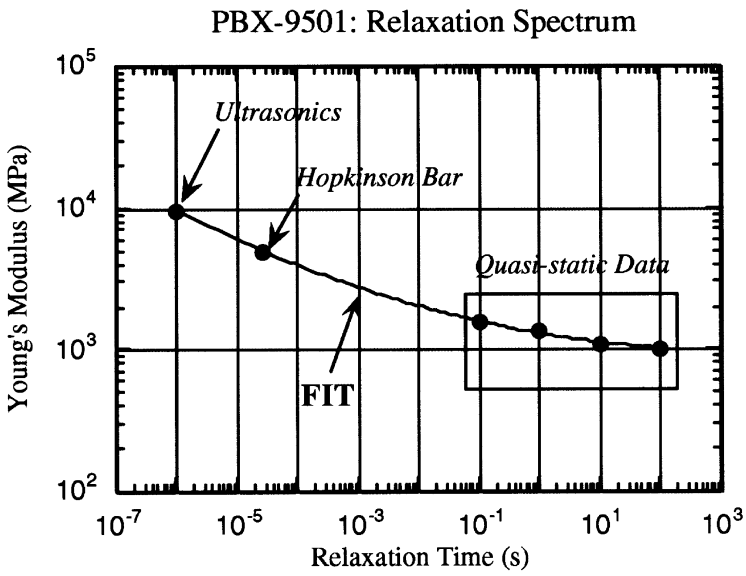

Fig. 4. The least squares fit to the Young's modulus versus relaxation time data for PBX-9501.

Table 1. *Cracking Parameters*

ν	a	m	c_0	v_{max}	K_0
0.3	0.001 m	10	0.00003 m	300 m/s	5×10^5 Pa$\sqrt{m}$

Table 2. *Shear Moduli for the Maxwell Elements*

G^1 (Pa)	G^2 (Pa)	G^3 (Pa)	G^4 (Pa)	G^5 (Pa)
9.440×10^8	1.738×10^8	5.212×10^8	9.085×10^8	6.875×10^8

Table 3. *Relaxation Parameters*

$1/\tau^1$	$1/\tau^2$	$1/\tau^3$	$1/\tau^4$	$1/\tau^5$
0	7.32×10^3 s	7.32×10^4 s	7.32×10^5 s	2.00×10^6 s

there is a statistical distribution of randomly oriented microcracks in the HMX material.

The hot-spot scale is such that the crack appears infinite in extent compared to the thermal influence. it is assumed that if the shear stress exceeds a static friction

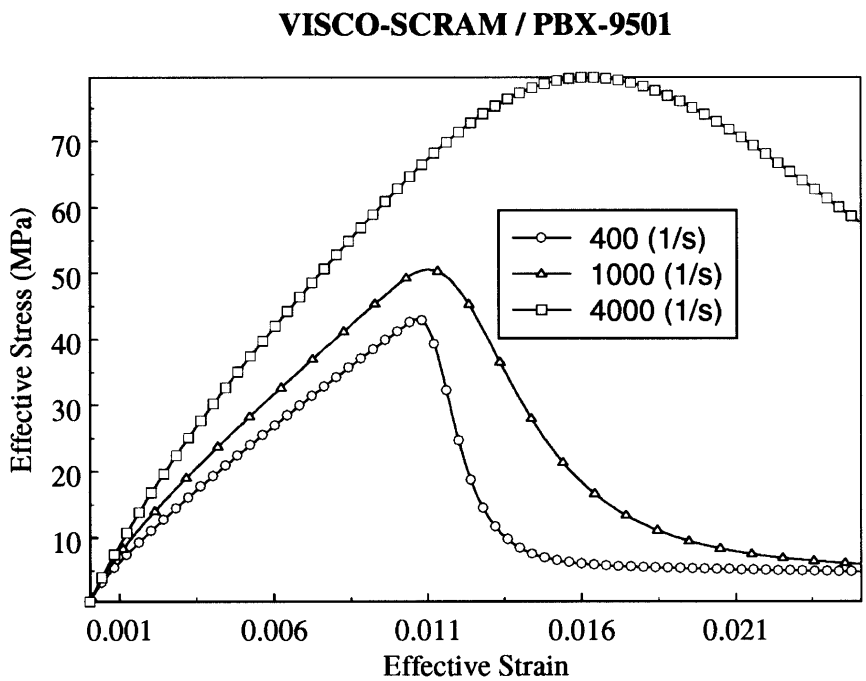

Fig. 5. Visco SCRAM response, PBX-9501, uniaxial stress.

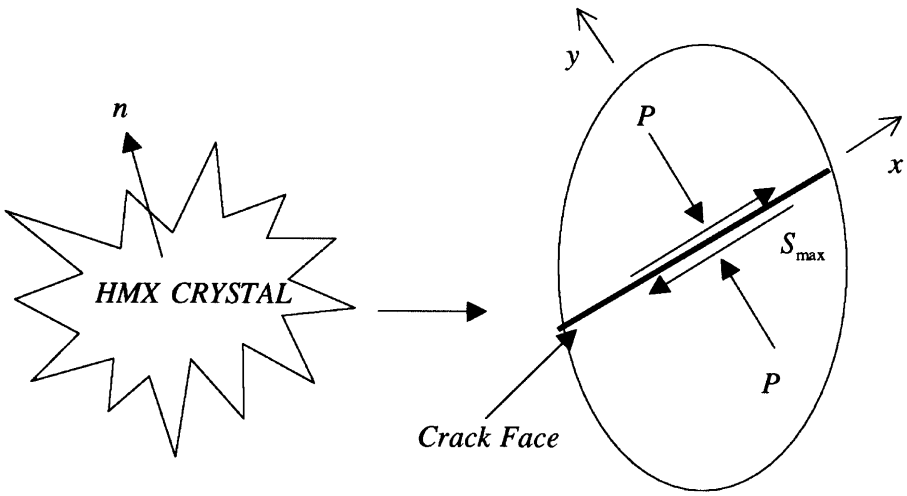

Fig. 6. The hot-spot model showing friction generated heat by the deviatoric stress on a plane normal to the direction of the maximum (principal) deviatoric strain rate.

Table 4. *Properties of HMX*

k_i	C_i	ρ_i	ΔH	Z	E/R
0.5	1.2×10^3	1.81×10^3	5.5×10^6	5×10^{19}	2.652×10^4

coefficient, the adjacent crack faces will slip and the work done on the slipping faces will generate heat. An energy balance on the model in Fig. 6 gives the modified Frank-Kamenetskii (1942) equations that govern the one dimensional heat transfer near the crack face

$$\frac{\partial}{\partial y}\left(k_f\frac{\partial T}{\partial y}\right)+\rho_f\Delta HZ\,\mathrm{e}^{\frac{E}{RT}}+\mu p\frac{\partial v_x}{\partial y}=\rho_f C_f\frac{\partial T}{\partial t},\quad l_f\geqslant y\geqslant 0 \tag{6}$$

$$\frac{\partial}{\partial y}\left(k_s\frac{\partial T}{\partial y}\right)+\rho_s\Delta HZ\,\mathrm{e}^{\frac{E}{RT}}=\rho_s C_s\frac{\partial T}{\partial t}. \tag{7}$$

Notice that here we are treating the hot-spot as having a length scale of l_f (to be determined), in extent and the frictional heat generation is volumetric, over the hot-spot volume. In eqns (6) and (7), term 1 is the heat conducted away from the hot-spot, term 2 is the chemical heat generation per unit volume, and the right hand side is the heat stored in the region of hot-spot influence. The variables in these equations are defined as:

T = absolute temperature (K),
k_i = thermal conductivity in material (W/(m−K)),
C_i = heat capacity in material (J/(kg−K)),
ρ_i = mass density in material (kg/m^3),
ΔH = heat of detonation (J/kg),
Z = a pre-exponential factor (1/s),
E = Arrhenius activation energy (kJ/mole),
R = universal gas constant (cal/(K−mole)),
t = time (s).

The properties used in this model for HMX are given in Table 4.

In addition, the model includes the latent heat of fusion during melt/resolidification, using the equivalent enthalpy method (Bonnett and Butler, 1996). A micro-crack is assumed to always exist normal to the direction of the maximum principal deformation rate in each element. Thus, the maximum principal deformation rate and its direction is found within each element from the strain rate tensor. The deviatoric stress is found on a plane normal to this direction, and checked to see if the value exceeds the value of $\mu_s p$, where μ_s is the static coefficient of friction, and p is the compressive pressure (if p is positive, the crack is assumed to be open and no heat is

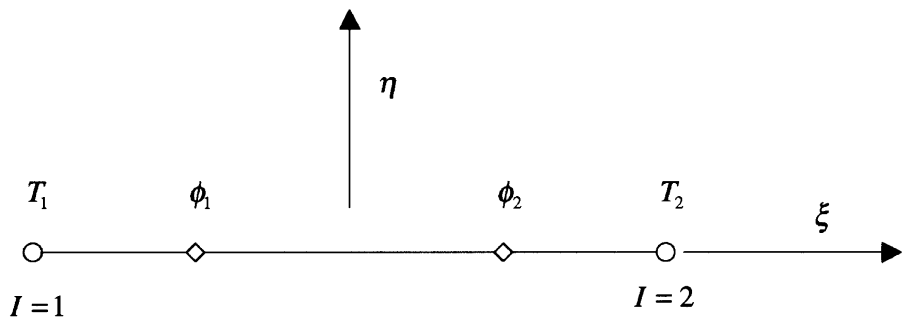

Fig. 7. The one dimensional heat transfer element.

generated). if the maximum shear stress on this plane exceeds this value, the crack is assumed to slip, and generates heat at the rate of

$$\mu p \frac{\partial v_x}{\partial y},$$

where μ is the dynamic value of the friction coefficient.

4.1. *Solution of the modified Frank-Kamenetskii Equations*

Equations (6) and (7) must be solved in each element at each time step. Dienes (1996) uses a finite difference technique. Here, in the interest of efficiency and accuracy, we use a weighted residual approach, which is, in effect, a one-dimensional finite element method. Figure 7 shows the temperature "element". The temperature is assumed to vary in the local coordinate as $T = H_1(\xi)T_1 + H_2(\xi)T_2 + H_3(\xi)\phi_1 + H_2(\xi)\phi_2$, where T_1 are the temperatures at the node I, and ϕ_1 are temperatures on the interior of the local domain, and H_1 are the interpolation functions. The geometry is assumed to map as $y = N_1 y_1 + N_2 y_2$, with the N_1 being the standard linear interpolation functions. The chemical heat generation within the domain is also assumed to interpolate in this manner, i.e.

$$\dot{Q}_{ch} = \sum_I N_I \dot{Q}_{chI}.$$

With this formulation, the gradients of temperature within the region $-1 \leqslant \varepsilon \leqslant 1$ can be resolved accurately because the interpolation functions for the temperatures, H_I, are cubic polynomials. The details of the development of the weighted residual equations are given in Appendix 1. The resulting matrix equations can be assembled into the form

$$\underline{\underline{K}}\,\underline{T} + \underline{\dot{Q}} = \underline{\underline{C}}\,\underline{\dot{T}},$$

that can be integrated in time using Euler backward time integration and Newton-Raphson iteration within the time-step for nonlinear material properties and tem-

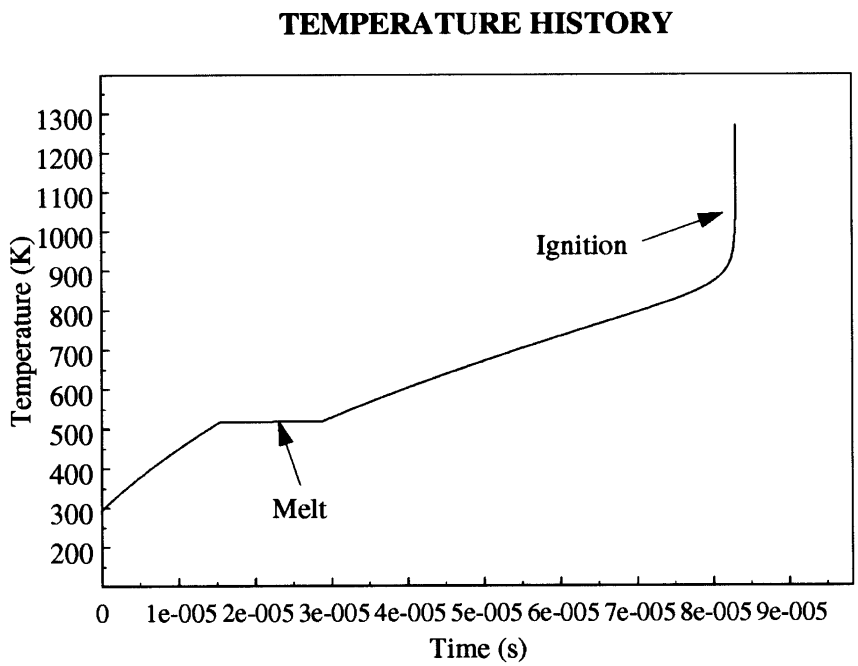

Fig. 8. Hot-spot predicted temperature-time history for a constant pressure and strain rate.

perature dependent loading. Details of this implementation are well known and can be found in any good finite element text (for example, Bathe, 1982).

The performance of the hot-spot model can be assessed separately from the implementation into the explicit finite element code by driving the model with a pressure and deviatoric deformation rate. For example, Fig. 8 shows the temperature vs time history for a hot-spot that is under a pressure of 1 GPa at a constant strain of 147,000 s^{-1}.

These values are typical of those calculated for a set of experiments that will be described. In Fig. 8, the temperature within the hot-spot is seen to increase until melt, remain almost constant during the melt period, and then to increase steadily until about 80 μs when the chemical heating produces a "runaway" temperature which is used as an ignition criterion.

Parameter studies were carried out using the hot-spot model to assess the sensitivity and performance of the model for later calibration against the data from experiments for impact and non-shock ignition of PBX-9501. For example, Fig. 9 shows the effect of varying the size of the hot-spot from 3 to 5 microns under a constant pressure and strain rate.

With increasing hot-spot size, the response will vary from non-ignition to ignition earlier in time. It should be emphasized that the hot-spot mechanism is the viscous heating over the volume of material adjacent to the statistically average crack (see eqn (6)), and that this volume parameter is calibrated by experiment.

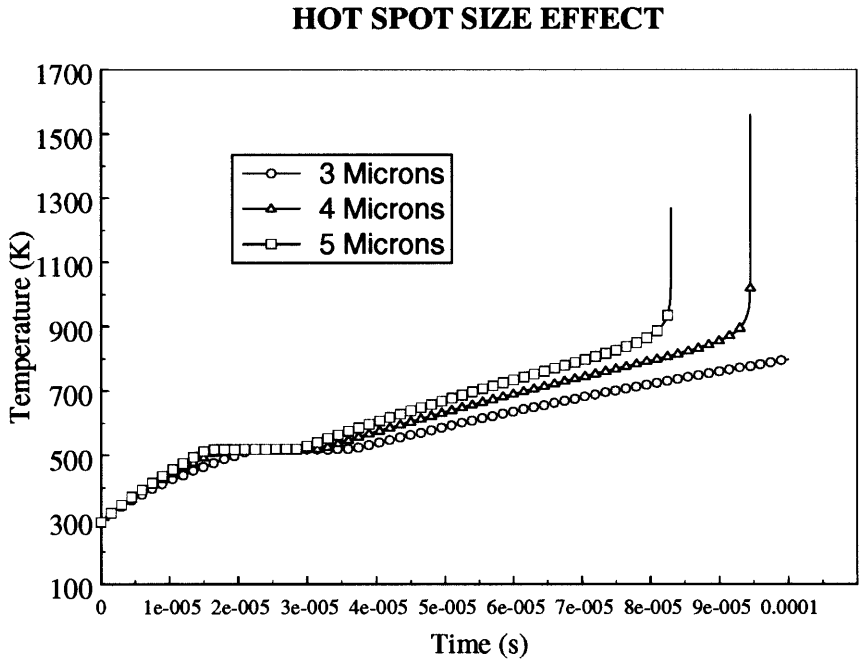

Fig. 9. The effect of hot-spot size on the temperature-time history for a constant pressure and strain rate.

Another study was conducted on the effect of "mesh extent". The boundary condition at the crack face is "no heat transfer" across the crack face because of symmetry. The calculation of the heat transfer away from the crack face should be carried out far enough spatially so that the calculated temperatures in the material are essentially the bulk temperatures of the material. The results of this study are shown in Fig. 10.

5. APPLICATIONS OF THIS MODEL TO EXPERIMENTS

Sets of experiments have been carried out to measure the non-shock ignition properties of PBX-9501 and are reported elsewhere (Asay, *et al.*, 1997). Essentially, a small rectangular piece of PBX-9501 is impacted with a plunger of known velocity and varying geometry, and the thermal response of the surface of the material as well as the in-plane displacement field at snapshots in time is measured during the response, the geometry being shown in Fig. 11. The in-plane displacements are measured using a speckle photography method developed at Los Alamos by Asay *et al.* (1997). The finite element calculational model shown in Fig. 12, faithfully reproduces the geometry of the experiments.

Figure 13 shows a qualitative comparison of the calculated surface displacement field and the measured one at 15 μs after impact for a 10-cm round-ended plunger. Figure 14 shows the quantitative comparison of the experimental surface displacement

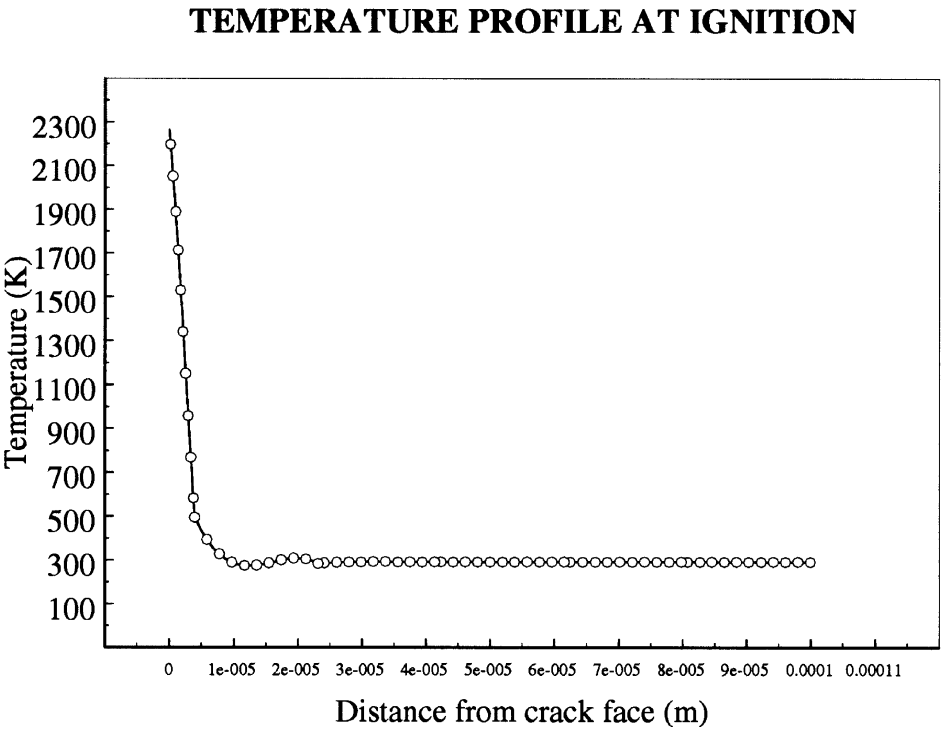

Fig. 10. Temperature vs distance from the crack-face at ignition.

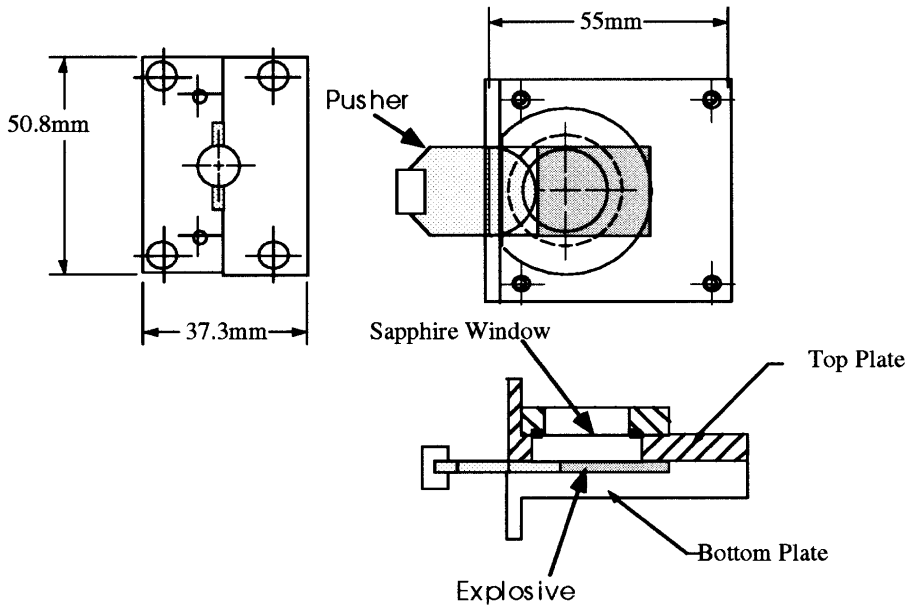

Fig. 11. Impact test geometry.

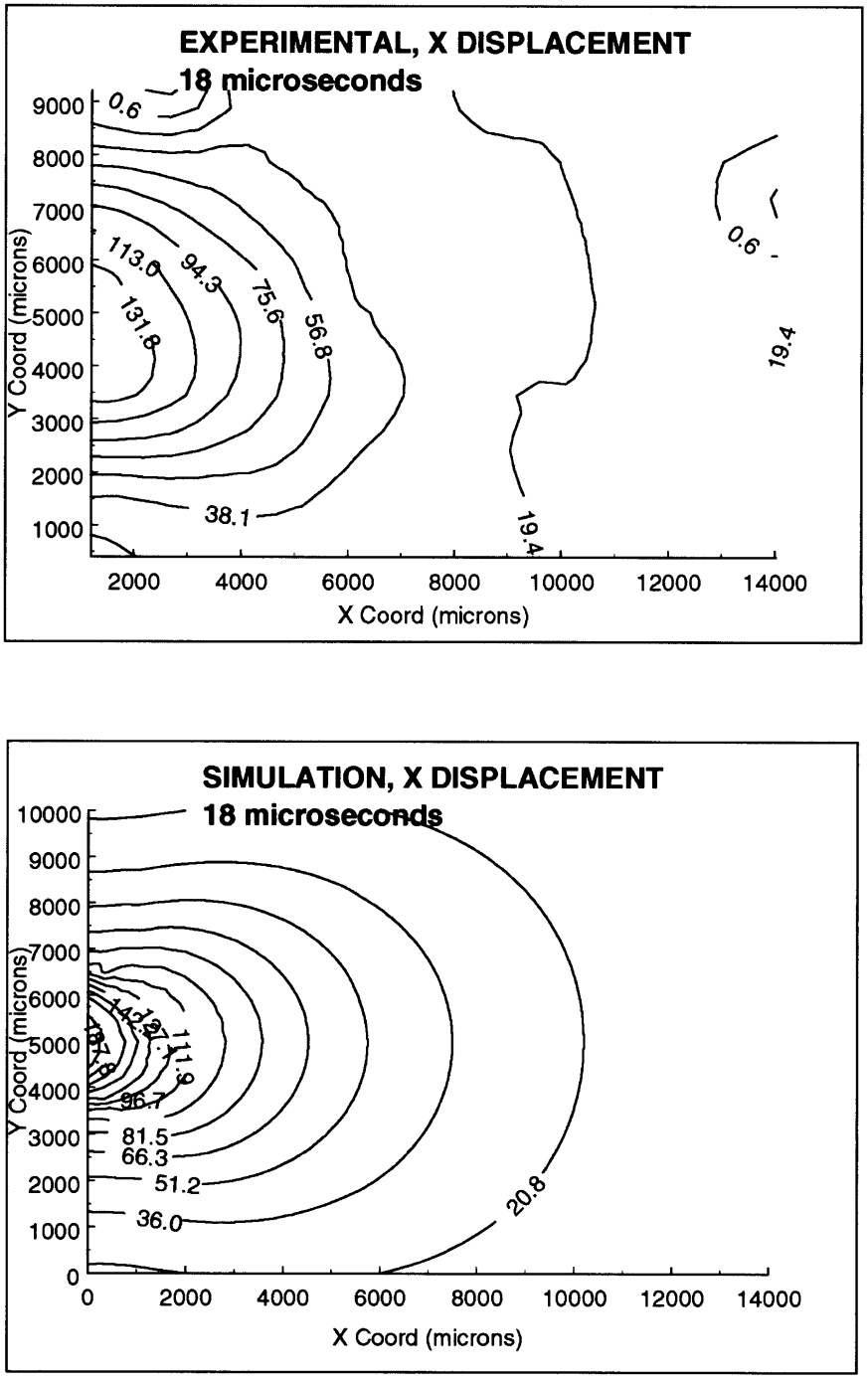

Fig. 14. A quantitative comparison of the calculated and experimentally measured surface displacement field.

field and the simulated one compared at 18 μs after impact. The comparisons are both qualitatively and quantitatively good, with the predicted displacement field being within the experimental accuracy of the measured one.

Figure 15 shows the results of a similar numerical simulation using a square-ended plunger. The simulation predicted ignition of the PBX-9501 at about 48 μs after impact. The surface temperatures indicated ignition at 100 μs after impact. At this point in time in our program, it is not clear whether actual ignition occurred earlier in the experiments or if the hotspot volumetric parameter is too large. Further experimental efforts are ongoing to clarify this point, but we believe one of the basic mechanisms needed to capture the mechanically induced ignition is in place. Furthermore, with this additional experimental insight and calibration, the model will be very useful in safety assessments.

6. CONCLUSIONS

A constitutive model for a high-explosive material (PBX-9501) has been developed that shows much promise in simulating the mechanical response and non-shock ignition prediction of this material. This model has been implemented into an explicit finite element program that is commonly used at Los Alamos in safety studies of systems that contain this material. The authors believe that this model and the experimental effort for calibration and verification of the predictions will be a very useful tool for safety studies aimed at preventing undesirable dispersion of Pu. The authors further believe that the methodology used in developing the model for this material can be used as a guide for developing similar models for other energetic materials.

ACKNOWLEDGEMENTS

The authors would like to acknowledge the very helpful discussion of the SCRAM model with John Dienes, T-14, Los Alamos National Laboratory. Most of the data presented in Fig. 4 are from unpublished measurements. In particular, the authors are grateful to G. T. (Rusty) Gray, MST-8, Los Alamos National Laboratory for the Hopkinson bar data taken in 1996, and D. A. Wiegand, Picatinny Arsenal, for providing the quasistatic measurements in 1996.

REFERENCES

Addessio, F. L. and Johnson, J. N. (1990) A Constitutive Model for the Dynamic Response of Brittle Materials. *Journal of Applied Physics* **67,** 3275–3286.

Asay, B. W., Funk, D. J., Henson, B. F. and Laabs, G. W. (1997) Speckle Photography During Dynamic Impact of an Energetic Material User Laser Induced Fluorescence. *Journal of Applied Physics* **82,** 1093–1099.

Bathe, Klaus-Jurgen (1982) *Finite Element 'Procedures in Engineering Analysis*. Prentice-Hall, Inc., Englewood Cliffs, New Jersey, 07632.

Bonnett, D. L. and Butler, P. B. (1996) Hot-Spot Ignition of Condensed Phase Energetic Materials. *Journal of Propulsion and Power* **12,** 680–690.

Dienes, J. K. (1996) A Unified Theory of Flow, Hot Spots, and Fragmentation with an Application to Explosive Sensitivity, In *High-Pressure Shock Compression of Solids II* ed. Lee Davison *et al.*

Dienes, J. K. (1984) Frictional Hot-spots and Propellant Sensitivity. *Proc. Mat. Res. Soc. Symp.* **24,**.

Field, J. E., Swallowe, G. M. and Heavens, S. N. 91982) Ignition Mechanisms of Explosives During Mechanical Deformation. *Proc. R. Soc. Lond. A* **382,** 231–244.

Field, J. E., Bourne, N. K., Palmer, S. J. P. and Walley, S. M. (1992) Hot-spot Ignition Mechanisms for Explosives and Propellants. *Phil. Trans. R. Soc. Lond. A* **339,** 269–283.

Field, J. E. (1992) Hot Spot Ignition Mechanisms for Explosives. *Acc. Chem. Res.* **25,** 489–496.

Frank-Kamenetskii, A. A. (1942) On the Mathematical Theory of Thermal Explosions. *Acta Physicochimica* URSS, Vol. XVI, No. 5–6, pp. 357–361.

Green, L. G., James, E., Lee, E. L., Chambers, E. S., Tarver, C. M., Westmorland, C., Weston, A. M. and Brown, B. (1981) Delayed Detonation in Propellants from Low Velocity Impact. In *Proc. 7th Symposium on Detonation* ed. J. M. Short. Annapolis, Md.

Howe, P. M., Gibbons, G. Jr. and Webber, P. E. (1985) An Experimental Investigation of the Role of Shear in Initiation of Detonation by Impact. In *Proc. 8th Symposium on Detonation*, Albuquerque, NM.

Jensen, R. C., Blommer, E. J. and Brown, B. (1981) An Instrumented Shotgun Facility to Study Impact Initiated Explosive Reactions. In *Proc. 7th Symposium on Detonation*, ed. J. M. Short, Annapolis, Md.

Maple, V. (1997) Software marketed by the Waterloo Maple, Inc, 450 Phillip Street, Waterloo, ON, Canada N2L 5J2.

Olinger, B. (1982) *Los Alamos Shock Wave Profile Data*, ed. C. E. Morris, pp. 280. UC Press, Berkeley.

Whirley, R. G. and Engelmann, B. E. (1993) *DYNA3D—A Nonlinear, Explicit, Three-Dimensional Finite Element Code for Solid and Structural Mechanics User Manual.* Lawrence Livermore National Laboratory, UCID-19592, Revision.

APPENDIX I

The Weighted Residual Equations for the Hot-spot Model

Referring to Fig. 7, the temperature within the local isoparametric domain $-1 \leqslant \bar{x}i \leqslant 1$ is given by $T = H_1(\xi)T_1 + H_2(\xi)T_2 + H_3(\xi)\phi_1 + H_4(\xi)\phi_2$, (with ϕ_i being internal node temperatures) where

$$H_1 = -\tfrac{1}{6} + \tfrac{1}{6}\xi + \tfrac{2}{3}\xi^2 - \tfrac{2}{3}\xi^3$$

$$H_2 = \tfrac{2}{3} - \tfrac{4}{3}\xi - \tfrac{2}{3}\xi^2 + \tfrac{4}{3}\xi^3$$

$$H_3 = \tfrac{2}{3} + \tfrac{4}{3}\xi - \tfrac{2}{3}\xi^2 - \tfrac{4}{3}\xi^3.$$

$$H_4 = -\tfrac{1}{6} - \tfrac{1}{6}\xi + \tfrac{2}{3}\xi^2 + \tfrac{2}{3}\xi^3.$$

These shape functions may be developed by the standard method of assuming a polynomial form for each function and applying the conditions that the temperatures satisfy, field variable

compatibility at the nodes, where for this set, the interior points have been chosen to be $\xi = \pm 1/2$. The geometry is assumed to interpolate linearly, with the shape functions being

$$N_1 = \tfrac{1}{2}(1-\xi)$$
$$N_2 = \tfrac{1}{2}(1+\xi).$$

Equations (6) and (7) can be restated in the general from

$$\frac{\partial}{\partial y} k \frac{\partial T}{\partial y} + \dot{Q} = \rho C \frac{\partial T}{\partial t}$$

where $\dot{Q}$ represents the contribution of the heat generation per unit volume, either frictional and/or chemical. Then substituting the assumed shape functions for the temperature and geometry, we have the general statement that

$$\frac{\partial}{\partial y} k \frac{\partial (H_1 T_1 + H_2 T_2 + H_3 \phi_3 + H_4 \phi_4)}{\partial y} + N_I \dot{Q}_I - \rho C \frac{\partial (H_1 T_1 + H_2 T_2 + H_3 \phi_3 + H_4 \phi_4)}{\partial t} = e,$$

where e is the residual error because of the interpolation. We now require that the weighted residual error be zero at each point for which the temperature is given exactly by the interpolation scheme, that is, we require

$$\int_y H_I e dy = 0.$$

These are the element weighted residual equations and can be restated in matrix equation form

$$\left[\int_y H_J \frac{\partial}{\partial y} k \frac{\partial H_I}{\partial y} dy\right] \begin{Bmatrix} T_1 \\ T_2 \\ \phi_1 \\ \phi_2 \end{Bmatrix} + \left(\int_y H_J N_K \dot{Q}_K dy\right) - \left[\int_y H_J H_I dy\right] \begin{Bmatrix} \dot{T}_1 \\ \dot{T}_2 \\ \dot{\phi}_1 \\ \dot{\phi}_2 \end{Bmatrix} = 0,$$

where $I, J = 1.4$; $K = 1,2$, and the summation rule on repeated indices applies. Notice that for the chemical heating terms in both eqns (6) and (7), we have assumed that within the domain

$$-1 \leqslant \varepsilon \leqslant 1, \quad \dot{Q} = N_I \dot{Q}_I,$$

and

$$\dot{Q}_I = \rho \Delta H Z e^{\frac{-E}{RT_I}}.$$

In addition, in eqn (6) the frictional heating term for the hotspot volume is

$$\dot{Q}_I = \mu p \frac{\partial v_x}{\partial y} = \mu p \dot{e}_{\max},$$

with $\dot{e}_{\max}$ being the maximum principal value of the deviatoric strain rate tensor, $\dot{\varepsilon}_{ij}$, evaluated at the DYNA3D element integration point.

The Green-Gauss theorem (integration by parts for this 1-D expression) can be applied to each of the integrals in the "thermal stiffness" coefficient matrix such that the first term in the element weighted residual expression can be written as

$$\left[\int_y \frac{\partial H_J}{\partial y} k \frac{\partial H_I}{\partial y} dy\right] \begin{pmatrix} T_1 \\ T_2 \\ \phi_1 \\ \phi_2 \end{pmatrix} + \textit{non-essential flux boundary conditions}.$$

All integrals in the 4×4 coefficient matrices can be evaluated simply in closed form using a symbolic algebra such as Maple V (1997). The element matrix equations can also be assembled in Maple for the form $\underline{\underline{K}}\underline{T} + \dot{\underline{Q}} = \underline{\underline{C}}\dot{\underline{T}}$ and the resulting algebraic forms written as FORTRAN files for incorporation into the hot-spot subroutines that are used in the DYNA3D constitutive model. Because no numerical integration is required in the hot-spot routines, the constitutive model is very efficient.